PROCEEDINGS, TOUGH Symposium 2003
Lawrence Berkeley National Laboratory, Berkeley, California, May 12-14, 2003

Flow Instabilities During Injection of CO_2 into Saline Aquifers

Julio E. García and Karsten Pruess
Earth Sciences Division
Lawrence Berkeley National Laboratory
Berkeley, CA, 94720
jegarcia@lbl.gov

ABSTRACT

Injection of carbon dioxide (CO_2) into saline aquifers has been proposed as a means to reduce greenhouse gas emissions (geological carbon sequestration). The injection process can be classified as immiscible displacement of an aqueous phase by a less dense and less viscous gas phase. Under disposal conditions (supercritical CO_2) the viscosity of carbon dioxide can be less than the viscosity of the aqueous phase by a factor of 15. Because of the lower viscosity, the CO_2 displacement front will have a tendency towards instability so that waves or rounded lobes of saturation may appear and grow into fingers that lead to enhanced dissolution, bypassing, and possibly poor sweep efficiency.

This paper presents an analysis, through high-resolution numerical simulations, of the onset of instabilities (viscous fingering) during injection of CO_2 into saline aquifers. We explore the influence of viscosity ratio, relative permeability functions, and capillary pressure on finger growth and spacing. In addition, we address the issues of finger triggering, convergence under grid refinement and boundary condition effects. Simulations were carried out on scalar machines, and on an IBM RS/6000 SP (a distributed-memory parallel computer with 6080 processors) with a parallelized version of `TOUGH2`.

INTRODUCTION

The injection process of carbon dioxide (CO_2) into saline aquifers can be classified as immiscible displacement of an aqueous phase by a less dense and less viscous gas phase. Because of the lower density and viscosity of CO_2 compared to water, the injection of CO_2 will have a tendency to produce hydrodynamic instabilities, leading to viscous fingering and gravity override. In order to avoid adverse effects from CO_2 separating into liquid and gas phases in the injection line, geological disposal of CO_2 would be made at supercritical pressures. The critical point of CO_2 is at $P_{crit} = 73.82$ bar, $T_{crit} = 31.04$ ^{o}C (Vargaftik et al., 1996), so that minimum aquifer depths of approximetely 800 m would be required to sustain a supercritical pressure regime.

Figure 1 shows the calculated CO_2 viscosity profile and the corresponding viscosity ratio (μ_{H_2O}/μ_{CO_2}) up to a depth of 2000 m. For this calculation a temperature gradient of $3^oC/100\ m$ and surface temperature of $10\ ^oC$ was assumed. Below 800 m the viscosity contrast between carbon dioxide and water is moderate with a viscosity ratio ranging from 22 at 800 m, to 10 at 2000 m.

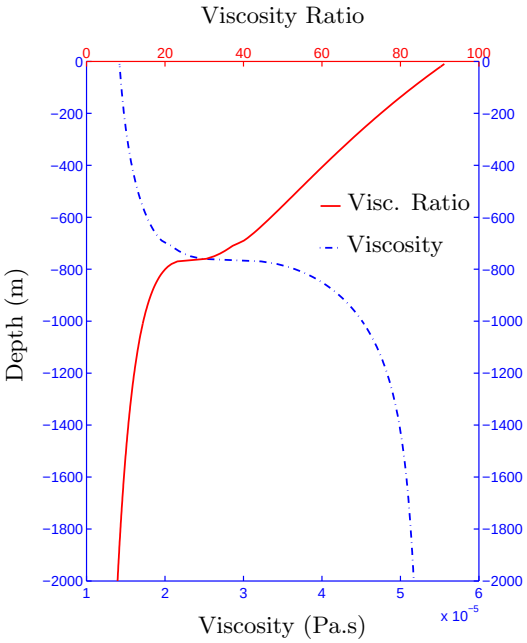

Figure 1: CO_2 viscositiy and viscosity ratio $\frac{\mu_{H_2O}}{\mu_{CO_2}}$.

In general, the displacement of a fluid by a less viscous one leads to the creation of fingers (viscous fingering) of low viscosity fluid penetrating the high viscosity fluid (Homsy, 1987). Mechanisms of viscous fingering and fluid displacements in porous media have been experimentally described by the early work of Hill (1952), van Meurs (1957), Saffman and Taylor (1958) and Chuoke et al. (1959).

Viscous fingering has been extensively studied for the case of miscible displacement. Sahimi (1993) and Homsy (1987) provided excellent reviews of the theory of viscous fingering in porous media. Zimmerman and

Homsy (1992) studied the effects of viscosity contrast and dispersion in three-dimensional finger propagation. Tchelepi and Orr (1994) addressed issues of viscous fingering with high-resolution two- and three-dimensional simulations of flow in homogeneous and heterogeneous porous media. More recently, De Wit and Homsy (1999a,b) studied viscous fingering in reaction-diffusion systems. Pankiewitz and Meiburg (1999), Ruith and Meiburg (2000) and Camhi et al. (2000) performed high resolution numerical simulations of miscible displacements with gravity override. On the other hand only a few previous numerical studies have examined viscous fingering due to immiscible displacement in porous media. Christie (1989) and Blunt et al. (1992) performed a series of viscous fingering simulations for compositional and immmiscible flows to investigate the effect of instabilities on oil recovery.

The purpose of this paper is to provide better understanding of the onset of viscous fingering during immiscible displacement in porous media. In particular we are interested in the flow instabilities that may occur during injection of CO_2 into saline aquifers. The general view is that, no matter the injection conditions, because the viscosity ratio μ_{H_20}/μ_{CO_2} is larger than unity, hydrodynamic unstable displacement will occur. The previous misleading assertion is often based on a large amount of immiscible flow observations in Hele-Shaw cells, and on past porous media investigations based on the assumption that single-phase flow regions are separated by an abrupt macroscopic interface. The approximation that only one phase flows upstream of the front, and only the other flows downstream is not valid for real porous materials. Immiscible displacement in porous media is characterized by simultaneous flow of both phases. In this case, it is the total mobility ratio, the sum of the mobilities of the two phases behind the front divided by the sum ahead that dictates the frontal instability: ratios larger than unity indicate instability and less than unity, stability. Thus, it is not only the viscosity ratio that is crucial to assert the stability but its interplay with the relative permeability functions through the fluid mobilities.

Our analysis is based on two-dimensional (2D) high-resolution numerical simulations that imply the absence of gravity override; we do not consider hysteresis on relative permeability and capillary pressure. The simulations presented assume an air-like gas with CO_2 viscosity rather than CO_2 itself. This is of course a rough simplification of the real CO_2-H_2O system and does not accurately represent certain processes. For example, CO_2 dissolution into the water phase that is expected to counter the tendency for fingering is underestimated. Nevertheless, the onset of instabilities, finger width and growth can appropriately be studied using this approach.

MATHEMATICAL FORMULATION

Governing Equations

In this formulation we assume, (1) zero mass transfer between fluid phases, (2) negligible rock compressibility, (3) immiscible flow, (4) incompressible fluids, (5) zero sources and sinks, (6) multiphase flow extension of Darcy's Law and (7) all the dependent variables are volumetric averages over a representative elementary volume (REV) (Bear, 1972). Less restrictive assumptions will be made in the numerical simulations below.

Under assumption (1), the mass balance equation for each fluid phase α may be written as

$$\frac{\partial}{\partial t}(\phi \rho_\alpha S_\alpha) + \nabla(\mathbf{f}_\alpha) = 0 \tag{1}$$

where ρ_α is the density of phase α, S_α is the saturation of phase α and ϕ is the porosity, with $\alpha \equiv g$ for gas and $\alpha \equiv l$ for liquid; $\mathbf{f}_\alpha$ is the flux of phase α. The flux of each phase, $\mathbf{f}_\alpha$, is related to the pressure gradient in terms of an extension of Darcy's law.

$$\mathbf{f}_\alpha = \rho_\alpha \boldsymbol{v}_\alpha = -\rho_\alpha \frac{\mathbf{k} k_{r\alpha}}{\mu_\alpha} \nabla(P_\alpha - \rho_\alpha \mathbf{g}) \tag{2}$$

where $\boldsymbol{v}_\alpha$ is the volumetric flux of phase α, $\mathbf{k}$ is the intrinsic permeability tensor, $k_{r\alpha}$ is the relative permeability of phase α, and $\mathbf{g}$ is the gravitational vector (the vertical coordinate is oriented positive downward). The pressures of the two phases are related through the capillary pressure, $P_c = P_g - P_l$. Relative permeability functions and capillary pressure are assumed to be functions of phase saturations. This approach, although supported by an abundance of experimental data, is still subject of debate (Juanes, 2003; Yortsos and Huang, 1986). Equation 1 is subject to the constraint that the two fluids jointly fill the void space, $S_g + S_l = 1$.

Problem formulation

The flow system under consideration (Figure 2) consists of a two dimensional porous medium domain with a constant cross-sectional area. The porous medium is considered homogeneous and isotropic and the effects of gravity are neglected. The system is initially at uniform liquid saturation S_l and gas is injected along the left boundary. The top and bottom boundaries are initially assumed no flow boundaries, and the domain is considered sufficiently long in the x direction so that the system would be infinite-acting for the time periods simulated.

The governing flow equations 1-2 are a set of coupled, nonlinear partial differential equations. These basic equations can be mathematically manipulated into several alternate forms with choices of primary dependent variables (Binning and Celia, 1999). For simplicity, consider the unidirectional flow with constant porosity

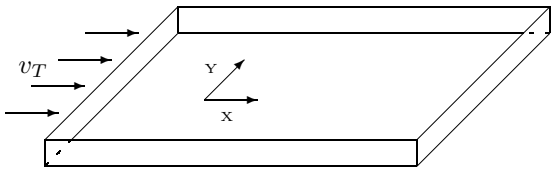

Figure 2: Schematic of flow system.

and fluid densities. Then the flow is described by the gas saturation equation:

$$\phi\frac{\partial S_g}{\partial t} + v_T\frac{\partial f_g}{\partial x} = +\frac{\partial}{\partial x}\left[\lambda_l\, f_g \frac{dP_c}{dS_g}\frac{\partial S_g}{\partial x}\right] \tag{3}$$

where $v_T = v_g + v_l$ is the total Darcy velocity (volumetric flux),

$$f_g = \frac{\lambda_g}{\lambda_T} \tag{4}$$

is the fractional flow of the gas phase (Buckley and Leverett, 1942),

$$\lambda_\alpha = \frac{k_{r\alpha}}{\mu_\alpha} \tag{5}$$

is the relative mobility of phase α, and $\lambda_T = \lambda_g + \lambda_l$ is the total mobility. In the absence of flow perturbations, a steady one-dimensional (1D) solutions develops moving along the direction of displacement, x, with a constant velocity, v. The velocity and shape of this front is dictated by the variation of relative permeabilities and capillary pressure as a function of saturation. For the typical displacement where capillary effects are assumed negligible, the saturation equation reduces to the Buckley-Leverett equation which may be solved analytically.

$$\phi\frac{\partial S_g}{\partial t} + v_T\frac{\partial f_g}{\partial x} = 0 \tag{6}$$

The Buckley-Leverett solution gives a saturation profile with a sharp front along the flow direction. When the initial saturation is uniform, the graphical approach developed by Welge (1952) can be used to determine the saturation front (Wu et al., 1990). As an example, the relative permeability functional forms determined by van Genuchten (1980) and Corey (1954) are used to derive the fractional flow function and the Buckley-Leverett Solution.

$$k_{rl} = \sqrt{S^*}\left\{1 - \left(1 - [S^*]^{1/m}\right)^m\right\}^2 \tag{7}$$

$$S^* = \frac{S_l - S_{lr}}{1 - S_{lr}} \tag{8}$$

$$k_{rg} = (1 - \hat{S})^2(1 - \hat{S}^2) \tag{9}$$

$$\hat{S} = \frac{S_l - S_{lr}}{1 - S_{lr} - S_{gr}} \tag{10}$$

For CO_2 and water, $\mu_g = 4.0 \cdot 10^{-5}$ N s m^{-2} and $\mu_l = 0.00075$ N s m^{-2} at $(T, P) = (82\ bar, 33\ ^oC)$, and relative permeability parameters $m = 0.85$, $S_{lr} = 0.25$, and $S_{gr} = 0.05$ we obtain the fractional flow curve f_g shown in Figure 3. Also shown in the figure is the tangent that originates at the initial gas saturation. The point of tangency defines the gas saturation at the displacement front and the slope of the Welge tangent gives the speed of the shock.

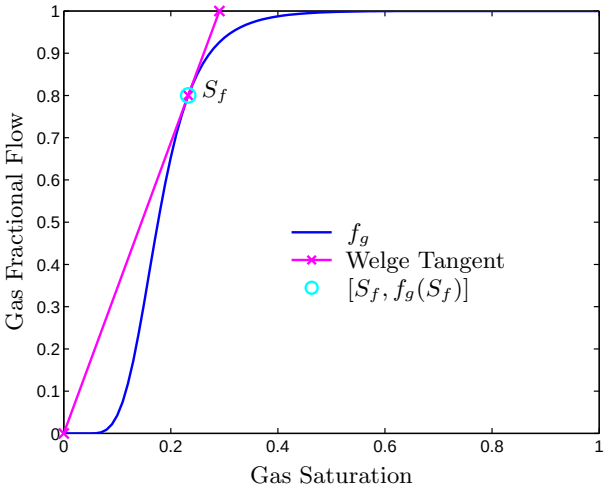

Figure 3: Fractional Flow Function.

Figures 4 and 5 show the total mobility and the Buckley-Leverett solution together with a numerical solution obtained with a front-tracking version `EOS3f` of `EOS3`. On the continuum level, the severity of the instability is controlled by the ratio of the total mobilities upstream and downstream of the front:

$$\lambda_{shock} = \frac{\lambda_T^{up}}{\lambda_T^{down}} \tag{11}$$

where upstream and downstream shock saturation and mobility values are denoted by S_g^{up} and S_g^{down}, λ_T^{up} and λ_T^{down}. Instabilities may occur when $\lambda_{shock} > 1$ while displacements whith $\lambda_{shock} \leq 1$ will proceed stably.

Figure 6 shows the variation of mobility shock (λ_{shock}), evaluated on the basis of a Buckley-Leverett shock front, with viscosity ratio. For illustration purposes we considered quadratic and cubic relative permeability functions as well as those given by Equations

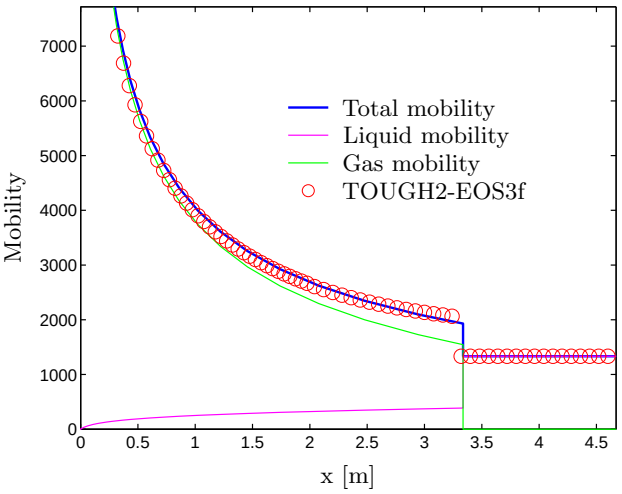

Figure 4: Buckley-Leverett solution for mobilities. Symbols represent the TOUGH2-EOS3f solution.

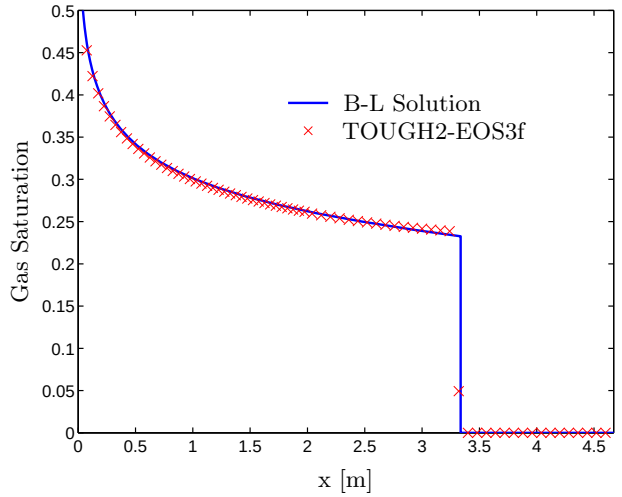

Figure 5: Buckley-Leverett solution for gas saturation. Symbols represent the numerical solution with front tracking (TOUGH2-EOS3f).

7 and 9 with $S_{lr} = 0.25$ and $S_{gr} = 0.05$. Mobility ratios are seem to be substantially smaller than viscosity ratios, indicating that flow instabilities in porous media will be weaker than for fluid displacements in "free" space. For CO_2 and H_2O (viscosity ratios between 10 and 100) the use of quadratic and cubic equations predicts always unstable displacements. Instability when using van Genuchten (1980) in conjunction with Corey (1954) relative permeablities depend on the shape factor m. For m values lower than 0.6, we expect stable displacements.

NUMERICAL IMPLEMENTATION

Viscous fingering was simulated using the `EOS3` module (two-phase flow of water and air) of the `TOUGH2` code

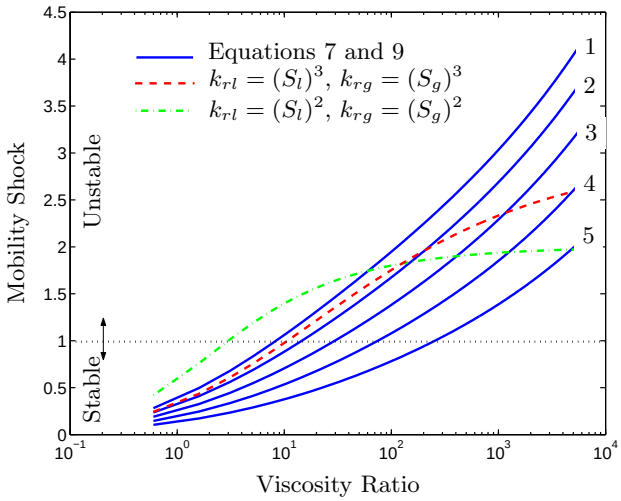

Figure 6: Stability of Immiscible displacement for different relative permeability functions. Curves 1, 2, 3, 4, and 5 refer to values of m=0.9, 0.8, 0.7, 0.6, 0.5 respectively in the van Genuchten (1980) relative permeability function.

(Pruess et al., 1999). Minor changes to this module were necessary in order to incorporate a set of fluid properties for different gas and liquid phases. A summary of the changes and a description of the computer platforms used is presented in Table 1.

Here, CO_2 is treated as an air-like gas as we do not attempt to capture all the fluid flow dynamics features due to the injection of CO_2 into water. Instead, our intent is to explore the possible outcome of instabilities when a fluid with CO_2 viscosity displaces water, and this can be accomplished with the modified version of `EOS3`. The reader is referred to Pruess and García (2002, 2003) and Pruess et al. (2003) for flow simulations for the system water, NaCl, carbon dioxide with more accurate representation of fluid properties.

Methods of triggering fingering

Several approaches can be used to trigger viscous fingers. Truncation and round-off errors seem to be the most tempting approach to perturb the displacement front and for that purpose one can reduce the convergence tolerance. Although successful in triggering fingers, this approach is not recommended as it does not allow to ascertain convergence under grid refinement. In our study we trigger fingers by one of two methods:

1. A random permeability field.

2. A finite amplitude perturbation of the inlet conditions during the first time step.

A mild random modifications of the permeability field, usually in the order of 4 % ($0.96 \times \mathbf{k} \leq \mathbf{k}_{mod} \leq 1.04 \times \mathbf{k}$), was made using the permeability modification

Table 1: Fluid Property Modules

Module	Platform	Description	Application
EOS3	A - B - C	Original EOS3 for single processor with minor changes to incorporate different fluid viscosities	1-D simulations to assess the stability of the front. Preliminary simulations in 2D
EOS3f	A - B	EOS3 with front tracking	Calculation of the B-L Solution
EOS3-MP	C	Parallel version of TOUGH2 (Zhang, 2003)	Sim. with more than 50,000 grid blocks

A: Pentium III (800 MHz) - Windows XP
B: Alpha-EV6.8AL (833MHz) - Tru64 UNIX V5.1
C: IBM-SP (1 Node=16 processors at 375 MHz and 32G memory, Max # of nodes=416) - AIX UNIX. Single processor version of EOS3 run at 375 MHz.

capabilities already incorporated in TOUGH2. Our simulations showed that the same finger structure is preserved whether the entire domain is perturbed or the permeability modification is localized in a strip after the injection boundary. Figure 7 shows that for a mobility shock, $\lambda_{shock} = 3.25$ fingers are triggered when the permeability is modified; the displacement is uniform otherwise.

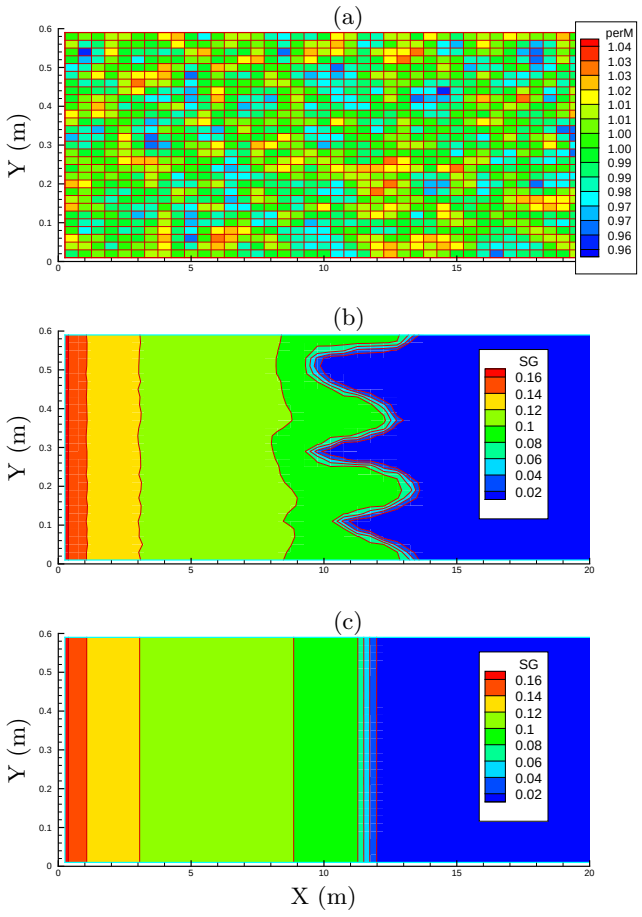

Figure 7: Viscous fingers are trigger (b) when a modified permeability field is used (a). No fingering occurs otherwise (c).

Convergence under grid refinement

Simulation results showed that finger growth and finger wave length are strongly affected by grid size. When the capillary diffusion effect is ignored in the gas saturation Equation 3, short wave length fingers are damped by the mesh size, and the solution obtained depends on the grid size no matter how much the grid is refined. When capillary effects are considered, it is possible to obtain solutions that converge under grid refinement. Our simulations show that for some cases an extremely fine grid (more than 100,000 grid blocks) is required (Figure 8). This requires simulation with the massive parallel scheme developed by Zhang (2003) and Wu et al. (2002).

Boundary effects

As mentioned before, the onset of instabilities is influenced by truncation and round-off errors. This problem becomes particularly relevant for no-flow boundary conditions. Figure 9a shows that fingers tend to grow more rapidly along such a boundary, creating an artificial, not realistic flow behavior. In order to avoid preferential flow along these boundaries we "glue" them together and link them by providing additional connections. The result is a two dimensional grid that is wrapped around the mantle of a cylinder, without no-flow boundaries.

Computer Performance

Our simulations showed that the overall computer performance depends primarily on the following aspects: (1) problem size (domain and gridblock size vs. injection rates); (2) mobility ratio; (3) the magnitude of the capillary effects. Single processor simulations proceed in a matched fashion on the three platforms. Finger evolution was tracked by obtaining printouts at specified times using the TOUGH2's keyword TIMES. This option is not available in the parallel version because the size of the problem implies very big output files. The progression of fingers at different times in the multiple processor version was captured by restarting the TOUGH2-MP run

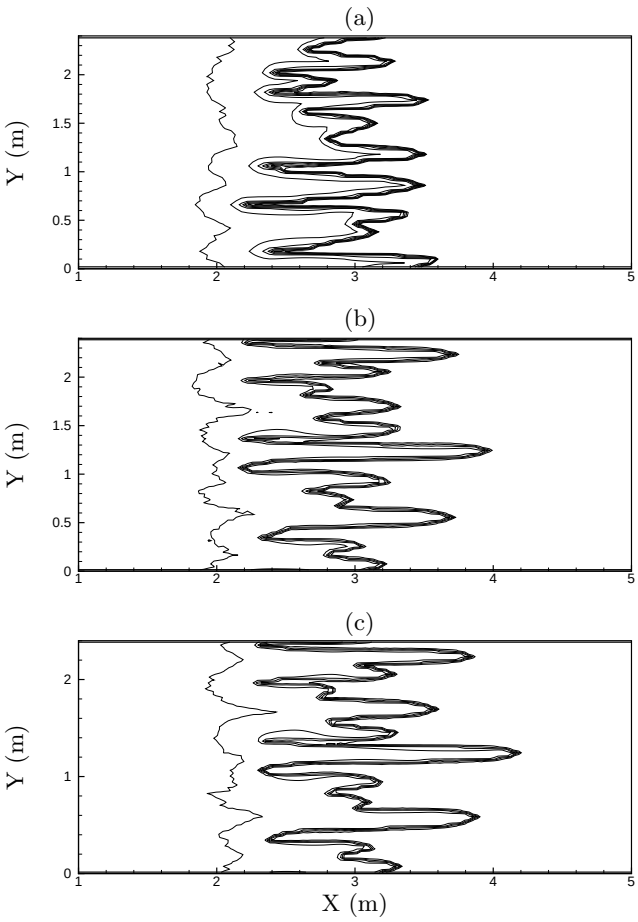

Figure 8: Grid Convergence (a) 15,480 (b) 61,920 (c) 141,120 Grid Blocks. Lines represent gas saturation contour levels with 0.02 increments, from $S_g = 0.02$ (right) to $S_g = 0.10$ (left).

providing the file SAVE generated in the previous run as file INCON. Results obtained from the single (Platform B) and multiple processor versions (Platform C) are almost identical. Minor differences in convergence behavior, time step size and number of iterations, are due to the use of different solvers. A 308×120 grid was used to compare the numerical results obtained with the two versions. In all the cases a similar finger structure is preserved. When using 16 processors, CPU times in the parallel implementation are reduced by a factor of 40. Because this problem is of modest size, the addition of more processors provides only a marginal gain in speed up. For larger problems though, the parallel-code simulations show a better than linear speedup until they reach a saturation point. Speedup here is defined to be relative to the performance with 16 processors. For additional information on the computer performance of the `TOUGH2` parallel version the reader is referred to Wu et al. (2002).

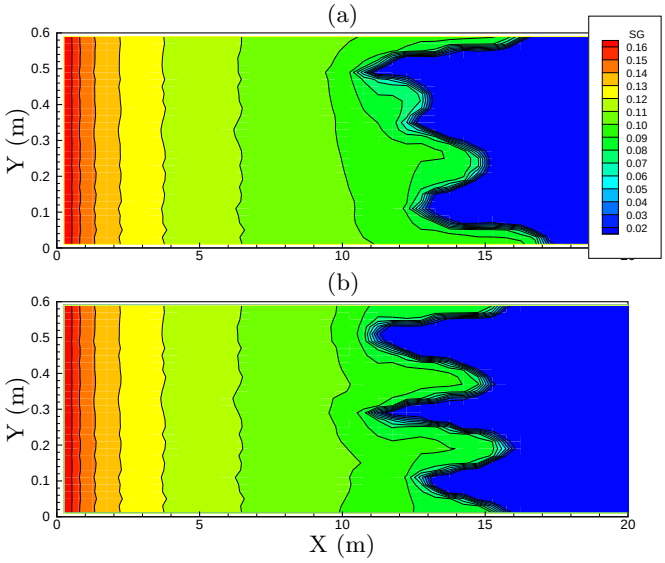

Figure 9: No-flow boundary conditions effect. (a) top and bottom no-flow boundaries. (b) top and bottom boundaries connected.

RESULTS AND APPLICATIONS

Chuoke et al. (1959) were the first to provide a theoretical analysis of the onset of fingering, using linear stability analysis. They assume that capillarity acts on a single macroscopic interface, in other words, that there is complete displacement of one fluid by other. An effective interfacial tension, σ^* was introduced to account for the pressure change across the interface.

Finger spacing

For the purpose of the analysis presented in this section we will consider the horizontal displacement of a gas-liquid interface as described by Chuoke et al. (1959). The region of the invading gas is labelled "1", the region of the invaded liquid "2". Because of the lower gas viscosity the displacement will be unstable. The frontal instabilities will continue to grow at a rate that is dependent on the wavelength of the perturbation. The expected finger spacing is given by the wave length of maximum growth rate,

$$\gamma_m = \sqrt{3}\gamma_c \tag{12}$$

where γ_c is the wave number of marginal stability, given for horizontal flow by

$$\gamma_c = 2\pi \left[\frac{\sigma^*}{\left(\frac{\mu_2}{k_2} - \frac{\mu_1}{k_1} \right) v} \right]^{1/2} \tag{13}$$

For the flow system under consideration (Figure 2) we

have $k_1 = k_2 = k$, so that Equation 12 can be written as

$$\gamma_m^2 = \frac{12\pi^2 k}{Ca} \tag{14}$$

Here, Ca is the local capillary number given for large viscosity ratio ($\mu_2 \gg \mu_1$) by

$$Ca = \frac{\mu_2 v}{\sigma^*} \tag{15}$$

The effective interfacial tension, σ^*, provides a link between the pore and the porous media continuum level. It is important to remind the reader that the previous analysis is based on the assumption that two macroscopic flow regions exist and furthermore that they are separated by an abrupt macroscopic interface. σ^* allows the pressure in the two regions across the interface to be related to the curvature of the interface. The effective interfacial tension is generally assumed to be directly proportional to the true interfacial tension σ.

In order to explore the validity of Chuoke's approximation we performed a series of numerical simulations with two hypothetical fluids, $\mu_l/\mu_g = 5500$, so that a high mobility shock can be obtained and maintained due to capillary effects. We use again the relative permeability functional forms given by equations 7 and 9. Figure 10 shows the expected finger width using Equation 14 for an intrinsic permeability of $k = 10^{-10}\ m^2$. The symbols represent the average finger width obtained from numerical simulations, showing good agreement between Equation 14 and simulated results. More analysis is required though to assess the validity of Chuoke's model on a more general continuum model.

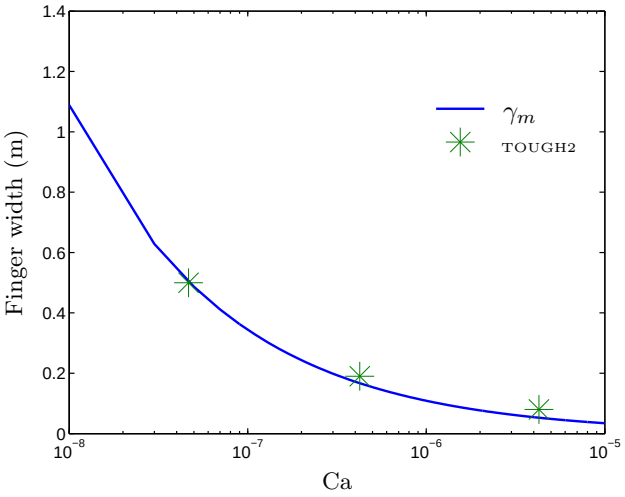

Figure 10: Finger Wave-Length.

Finger growth

Figure 11 shows gas saturations at three different times in a two-dimensional displacement obtained on a 616 × 240 grid. Viscous fingering is triggered by variations in the permeability with a maximum modification of 5 % ($0.95 \times \mathbf{k} \leq \mathbf{k}_{mod} \leq 1.05 \times \mathbf{k}$, with $\mathbf{k} = 10^{-10}$). Figure 12a shows the location of the saturation front ($X_f(t)$) calculated as a uniform displacement according to the Buckley-Leverett solution together with the absolute finger length ($\Omega(t)$) obtained from the simulation results at 11 times. The relative finger length is calculated as:

$$\omega(t) = \frac{\Omega(t)}{X_f(t)} \tag{16}$$

The relative finger length shown in Figure 12b increases at first, and later appears to reach an asymptotic value.

CONCLUDING REMARKS

This paper describes flow simulations exploring hydrodynamic instability during immiscible displacement in porous media. Simulation results show that TOUGH2 is capable of capturing viscous fingering when there is a displacement of a viscous fluid by a less viscous one. Furthermore, the preliminary results obtained show agreement with classic instability analysis of immiscible displacements in porous media (Chuoke et al., 1959). Capillary effects act to stabilize the displacement at higher wavelengths. Thus, for higher capillary numbers smaller finger widths are expected.

The simulations examined the injection of CO_2 into a domain originally saturated with water. For aquifer disposal conditions, the use of common relative permeability functions gives a mobility ratio less than unity ($\lambda_{shock} < 1$), resulting in a stable displacement. When quadratic and cubic relative permeability functions are used, or when extreme shape factors are applied to other conventional relative permeability functions such as the van Genuchten (1980), an unstable displacement may occur with moderate mobility ratios of up to 2.5. In addition, both capillary effects and dissolution of CO_2 in the aqueous phase will counter the tendency for fingering. Tchelepi and Orr (1994) found that, for miscible displacement in reservoirs, the distribution of permeability rather than hydrodynamic instability dominates fluid displacement. We expect that this will also be the case for CO_2 injection into saline aquifers. Low-viscosity CO_2 will find preferential flow paths easily and the heterogeneity structure of the aquifer will determine the extent of channelling and by-passing.

ACKNOWLEDGEMENTS

We are grateful to Keni Zhang for his help adapting the parallel version of TOUGH2 to the simulations presented in this paper. This work was supported by the US Department of Energy through the Office of Basic Energy Sciences under Contract No. DE-AC03-76SF00098.

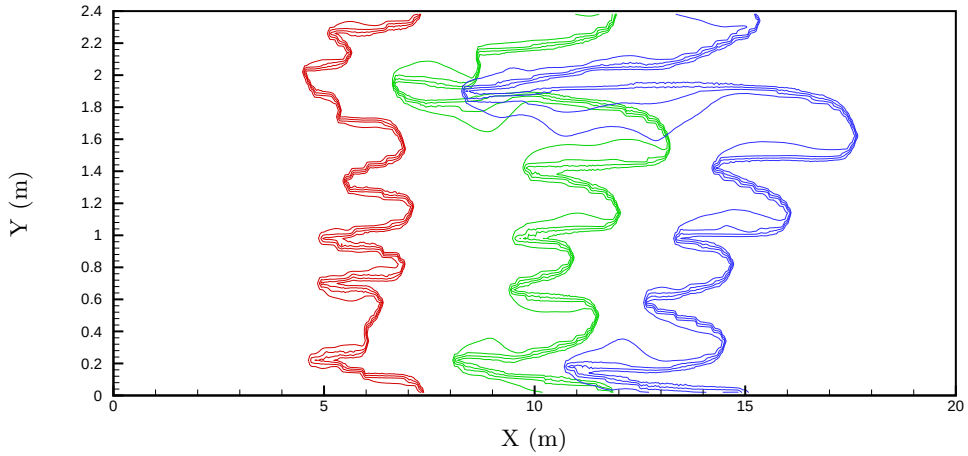

Figure 11: Finger Growth. Lines represent frontal gas saturation contour levels ($0.08 \geq S_g \geq 0.02$) at $T = (1.0 \times 10^7,\ 2.0 \times 10^7,\ 3.0 \times 10^7)$ *sec.*

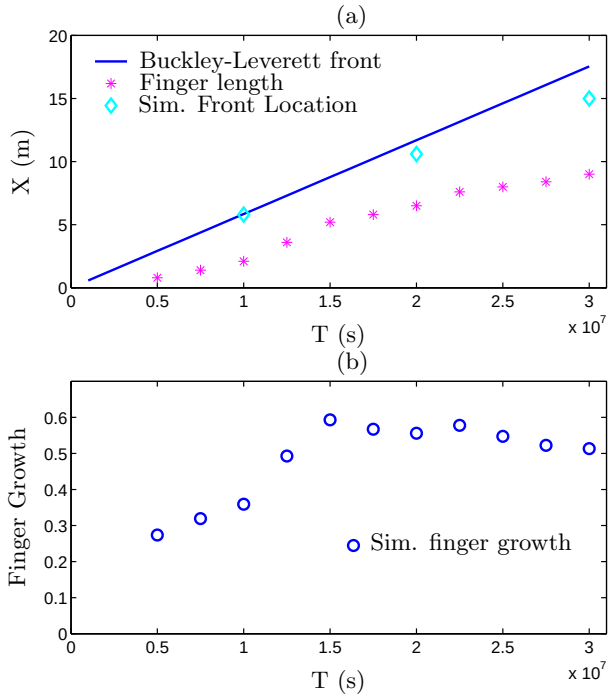

Figure 12: High-resolution simulation results for finger growth.

References

Bear, J. (1972). *Dynamics of Fluids in Porous Media*. Dover Publications, Inc., New York, NY.

Binning, P. and Celia, M. A. (1999). Practical implementation of the fractional flow approach to multi-phase flow simulation. *Adv. Water Resour.*, 22(5):461–478.

Blunt, M. J., Barker, J. W., Rubin, B., Mansfield, M., Culverwell, I. D., and Christie, M. A. (1992). A predictive theory for viscous fingering in compositional displacement. In *SPE/DOE Eigth Symposium on Enhanced Oil Recovery*, Tulsa, Oklahoma. SPE 24129.

Buckley, S. E. and Leverett, M. C. (1942). Mechanism of fluid displacement in sands. *Petrol. Trans.* AIME, 146:107.

Camhi, E., Mieburg, E., and Ruith, M. (2000). Miscible rectilinear displacements with gravity override. Part 2. Heterogeneous porous media. *J. Fluid Mech.*, 420:259–276.

Christie, M. A. (1989). High-resolution simulations of unstable flows in porous media. *SPE Reserv. Eng.*, pages 297–303. SPE 16005.

Chuoke, R. L., van Meurs, P., and van der Poel, C. (1959). The instability of slow, immiscible, viscous liquid-liquid displacements in permeable media. *Petrol. Trans.* AIME, 216:188–194.

Corey, A. T. (1954). The interrelation between gas and oil relative permeabilities. *Producers Monthly*, pages 38–41.

De Wit, A. and Homsy, G. M. (1999a). Nonlinear interactions of chemical reactions and viscous fingering in porous media. 11(5):949–951.

De Wit, A. and Homsy, G. M. (1999b). Viscous fingering in reaction-diffusion systems. *J. Chem. Phys.*, 110(17):8663–8675.

Hill, S. (1952). Channelling in packed columns. *Chem. Eng. Sci.*, I(6):247–253.

Homsy, G. M. (1987). Viscous fingering in porous media. *Ann. Rev. Fluid Mech.*, 19:271–311.

Juanes, R. (2003). *Displacement theory and multiscale numerical modeling of three-phase flow in porous media*. PhD thesis, University of California at Berkeley.

Pankiewitz, C. and Meiburg, E. (1999). Miscible porous media displacement in the quarter five-spot configuration. Part 3. Non-monotonic viscosity profiles. *J. Fluid Mech.*, 388:171–195.

Pruess, K. and García, J. E. (2002). Multiphase flow dynamics during CO_2 disposal into saline aquifers. *Environmental Geology*, 42(2-3):282–295.

Pruess, K. and García, J. E. (2003). Solutions of test problems for disposal of CO_2 in saline aquifers. Technical Report LBNL-51812, Lawrence Berkeley National Laboratory, Berkeley, CA.

Pruess, K., Oldenburg, C., and Moridis, G. (1999). TOUGH2 user's guide, version 2.0. Technical Report LBNL-43134, Lawrence Berkeley National Laboratory, Berkeley, California.

Pruess, K., Xu, T., Apps, J., and Garcia, J. (2003). Numerical modeling of aquifer disposal of CO_2. *Soc. Pet. Eng. J.*, pages 49–60. SPE 83695.

Ruith, M. and Meiburg, E. (2000). Miscible rectilineas displacements with gravity override. Part 1. Homogeneous porous medium. *J. Fluid Mech.*, 420:225–257.

Saffman, P. G. and Taylor, S. G. (1958). The penetration of a fluid into a porous medium or Hele-Shaw cell containing a more viscous liquid. *Proc. Roy. Soc. London Series A.*, 245:296–305.

Sahimi, M. (1993). Flow phenomena in rocks: from continuum models to fractals, percolation, cellular automata, and simulated annealing. *Reviews of Modern Physics*, 65(4):1393–1537.

Tchelepi, H. A. and Orr, F. M. (1994). Interaction of viscous fingering, permeability heterogeneity, and gravity segregation in three dimensions. *SPE Reserv. Eng.*, pages 266–271. (SPE 25235).

van Genuchten, M. T. (1980). A closed-form equation for predicting the hydraulic conductivity of unsaturated soils. 44:892–898.

van Meurs, P. (1957). The use of transparent three-dimensional models for studying the mechanism of flow processes in oil reservoirs. *Petrol. Trans.* AIME, 210:295–301.

Vargaftik, N. B., Vinogradov, Y. K., and Yargin, V. S. (1996). *Handbook of Physical Properties of Liquids and Gases*. Begell House, New York, third edition.

Welge, H. J. (1952). A simplified method for computing oil recovery by gas or water drive. *Petrol. Trans.* AIME, 195:91–98.

Wu, Y.-S., Pruess, K., and Chen, Z. X. (1990). Buckley-leverett in composite porous media. Technical Report LBL-28937, Lawrence Berkeley National Laboratory, Berkeley, California.

Wu, Y.-S., Zhang, K., Ding, C., Pruess, K., Elmroth, E., and Bodvarson, G. (2002). An efficient parallel-computing method for modeling nonisothermal multiphase flow and multicomponent transport in porous and fractured media. *Adv. Water Resour.*, 25:243–261.

Yortsos, Y. and Huang, A. B. (1986). Linear stability analysis of immiscible displacement Part 1 - Simple basic flow profiles. *SPE Reserv. Eng.*, pages 378–390. (SPE 12692).

Zhang, K. (2003). User's manual for TOUGH2_MP vesion 1.0. Technical report, Lawrence Berkeley National Laboratory.

Zimmerman, W. B. and Homsy, G. M. (1992). Three-dimensional viscous fingering: A numerical study. *Phys. Fluids A*, 4(9):1901–1914.